Wavelength-Tunable and OAM-Switchable Ultrafast Fiber Laser Enabled by Intracavity Polarization Control

Haifeng Hu , Zhuo Chen, Qian Cao , and Qiwen Zhan , *Senior Member, IEEE*

Abstract—**Ultrafast laser that directly emits vortex beam has broad application prospects in many research fields and applications, such as telecommunication, bio-sampling and quantum information science. In this article, we demonstrate a wavelength-tunable and OAM-switchable ultrafast fiber laser enabled by intracavity polarization controlling elements. The mode-locked laser can emit vortex beam outputs with a topological charge of $l = +1$ or $l = -1$ and the center wavelength can be continuously tuned from 1015 nm to 1038nm. The obtained output pulse has a pulse energy of 3.3 nJ and a compressed pulse duration of 87 fs. Compared with previous results, this laser can emit OAM-switchable output with a shorter pulse duration and a broad wavelength tuning range. The concept of adding polarization control elements to a mode-locked fiber laser can be further expanded to build laser with more sophisticated and customizable outputs.**

Index Terms—**Lasers, optical amplifiers, and laser optics.**

I. INTRODUCTION

VORTEX beam with orbital angular momentum (OAM) has been widely studied in scientific researches and applications [1]. Having an azimuth phase term of $\exp(il\theta)$, vortex beam features a phase singularity in the beam center and a ring-like intensity profile. Due to the unique phase and intensity distribution, vortex beam has facilitated many applications such as material processing [2], [3], microscopic imaging [4], [5], optical tweezers [6], [7], [8], optical communication [9], [10] and quantum information processing [11].

To generate a vortex beam, researchers have developed various methods which include generating the vortex external to the laser cavity, or generating vortex internal to the laser cavity. In the first one, the vortex beam is generated externally to the laser cavity by programmable or customized photonic devices such as spatial light modulator (SLM) [12], metasurface [13], sub-wavelength grating [14], spiral phase plate [15] and q-plate [16]. These devices can convert the laser output, typically a fundamental Gaussian beam, into vortex beam. In the second one, vortex beam is directly emitted from the laser cavity. Since the photon within the vortex beam carries photonic OAM of $l\hbar$, such laser is also referred to as OAM laser. To modify the intracavity mode of a laser, scientists have been using intracavity amplitude filters, phase plates, deformable mirrors, and SLM to generate the favorable output mode from the laser [17]. Using fiber-based devices, scientists also demonstrate the direct generation of vortex beam from a fiber laser based on long-period fiber grating [18]. However, these lasers are mainly working in the continuous wave mode, which is not favorable for applications that need vortex beam with high peak power and short pulse duration, for example, material processing [19], [20], electron accelerations [21] and nonlinear optical microscopies [22]. Recently, research groups have built mode-locked OAM fiber laser using s-waveplate [23], q-plate [24], [25], [26], acousto-optic mode converter (AOMC) [27], offset splicing structure (OSS) with a two-mode fiber Bragg grating [28] and nonlinear loop mirror (NOLM) device [29]. In those realizations, the center wavelength of the OAM laser cannot be freely tuned.

Despite previous success in building OAM lasers, demonstration of laser that can directly emit wavelength-tunable and OAM-switchable ultrafast output is still lacking. Such OAM laser may find broad applications in telecommunications, biological sampling, and quantum information science. In this work, we demonstrate a wavelength-tunable and OAM-switchable mode-locked fiber laser enabled by intracavity polarization control elements. Pulsed vortex beam can be directly generated from this OAM laser. Inside the laser cavity, we use additional vortex wave plates (VWP) and quarter wave plates (QWP) for achieving modal conversion inside the laser. The orientation of these waveplates can be changed to generate vortex beam with a selective topological charge. The center wavelength of OAM

Haifeng Hu, Qian Cao, and Qiwen Zhan are with the School of Optical-Electrical and Computer Engineering, University of Shanghai for Science and Technology, Shanghai 200093, China, also with the Zhangjiang Laboratory, Shanghai 201204, China, and also with the Shanghai Key Lab of Modern Optical System, University of Shanghai for Science and Technology, Shanghai 200093, China (e-mail: hfhu@usst.edu.cn; cao.qian@usst.edu.cn; qwzhan@usst.edu.cn).

Zhuo Chen is with the School of Optical-Electrical and Computer Engineering, University of Shanghai for Science and Technology, Shanghai 200093, China (e-mail: 202310328@st.usst.edu.cn).
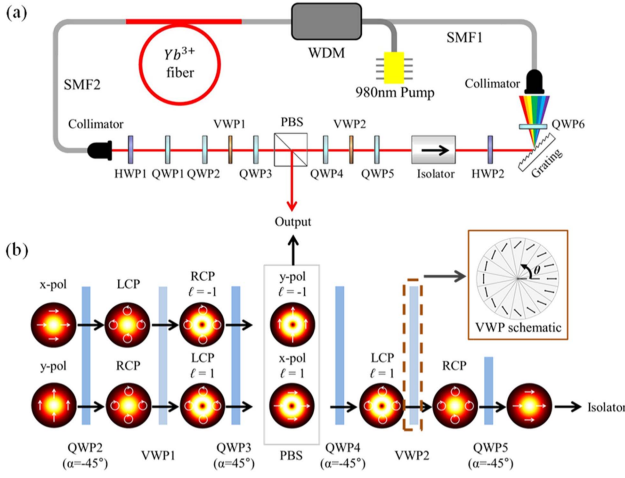
Fig. 1. Schematic and working principle of the mode-locked OAM laser. (a) The experimental setup of fiber laser generating optical vortex beams with orbital angular momentum. WDM: wavelength division multiplexer; HWP: Half-wave plate; QWP: Quarter-wave plate; PBS: Polarization beam splitter; VWP: Vortex wave plate. (b) The function of polarization control elements on x-polarized light (upper row) and y-polarized light (lower row); inset: Schematic of VWP.

laser can be continuously tuned from 1015 nm to 1038 nm while the mode-locking state is always retained. Compared with previous results [17], [18], [24], [29], we generate a wavelength-tunable and OAM-switchable mode-locked laser with a shorter pulse duration. The concept of this laser can be further expanded to build ultrafast lasers with a more sophisticated, customizable spatial profile for its output.

II. EXPERIMENTAL SETUP

Fig. 1(a) shows the schematic of the mode-locked OAM laser. The cavity has an all-normal-dispersion (ANDi) fiber laser structure [30], [31], [32]. The fiber part consists a 2.2 m single mode fiber (SMF1), a wavelength division multiplexer (WDM) for coupling $\lambda = 980$ nm pump light into the gain fiber, a 0.6 m double-cladding ytterbium-doped fiber, and a 2.8 m SMF2. The total length of the optical fiber is 5.6m, providing a net cavity dispersion of 0.11 ps^2. Both ends of the fiber are spliced with two fiber collimators that collimate the fiber beam into a 2mm beam in free space.

In the free space part, the total optical path length is 0.7m. One half wave plate (HWP1), two quarter wave plate (QWP1 and QWP6), and a polarization beam splitter (PBS) realize the nonlinear polarization evolution (NPE) inside the fiber. The angle of the wave plates is adjusted so that high-energy pulses can pass through PBS and keep circulating inside the cavity while low-energy pulses are reflected by PBS and become the laser output. These components can thus act as a virtual saturable absorber for the laser. A diffraction grating (600 lines/mm) is placed before QWP6 to couple the diffracted light back to fiber. The grating acts as a spectral filter for the laser, which helps self-start the mode-locking process. HWP2 is inserted before the grating for maximizing the efficiency. A free-space isolator is placed before HWP2 for ensuring the unidirectional propagation of light inside the laser.

To generate vortex beam inside the cavity, polarization control elements are introduced including two VWPs (VWP1, 2) and four QWPs (QWP2-5). The operation of polarization control elements on the oscillating beam is illustrated in Fig. 1(b). The first row shows the operation of these elements on x-polarized light and the second row shows the polarization operation on y-polarized light. When x-polarized light passes QWP2 ($\alpha = -45°$, α: The angle between the optical axis of the wave plate and the horizontal direction), it becomes left-circularly polarized (LCP). Then VWP1 converts it into a RCP vortex beam with a topological charge of $l = -1$. After QWP3 ($\alpha = 45°$), the beam becomes y-polarized and it is reflected by PBS as the laser output.

Meanwhile, y-polarized light becomes x-polarized vortex beam with $l = +1$ after QWP2, VWP1, and QWP3. It can pass through PBS and the subsequent QWP4, VWP2, and QWP5. These elements convert the beam back to a x-polarized Gaussian beam and the beam can continue circulating inside the laser. The inclusion of QWP4, VWP2, QWP5 is crucial for this laser because a fundamental Gaussian beam can be coupled back to the single-mode fiber with a significantly higher efficiency.

The mode transformation of the transverse beam can be expressed by the following Jones matrix calculation [33]. When an input light E_i passes through N polarization devices in sequence with their Jones matrix being G_1, G_2 …G_N. The transmitted output light E_t can be written as

$$E_t = G_N \ldots G_2 G_1 E_i \qquad (1)$$

An input light with x-polarization E_{x0} is converted into y-polarized after QWP2, VWP1 and QWP3. It is then reflected by PBS and becomes the laser output E_{Output}. Meanwhile, y-polarized input light E_{y0} is converted into x-polarized after all these polarization controlling elements and the light can continue to circulate inside the laser ring as E_2.

$$E_{Output} = G_{45°} G_v G_{-45°} E_{x0} \begin{bmatrix} 1 \\ 0 \end{bmatrix}$$

$$= E_{x0} \exp\left[-i\left(\frac{\pi}{2} - \theta\right)\right] \begin{bmatrix} 0 \\ 1 \end{bmatrix} \qquad (2)$$

$$E_2 = G_{-45°} G_v G_{-45°} G_{45°} G_v G_{-45°} E_{y0} \begin{bmatrix} 0 \\ 1 \end{bmatrix}$$

$$= E_{y0} \exp\left(-i\frac{\pi}{2}\right) \begin{bmatrix} 1 \\ 0 \end{bmatrix} \qquad (3)$$

Here, $\exp(i\theta)$ is the spiral phase factor for VWP, θ the azimuth angle, and the Jones matrices of polarization control elements are given in Table I.

III. EXPERIMENTAL RESULTS

In the experiment, the laser is mode-locked when the pump current reaches a threshold value of 400 mA. The mode-locking state is always retained even when a pump current of 1200mA is applied. Fig. 2 shows the characterization of the laser at a pump current of 500mA. Fig. 2(a) shows the spatial profile of the laser output after pulse compression, showing a typical ring-like profile of a vortex beam. The purity coefficient of the vortex

TABLE I
JONES MATRICES OF OPTICAL ELEMENTS

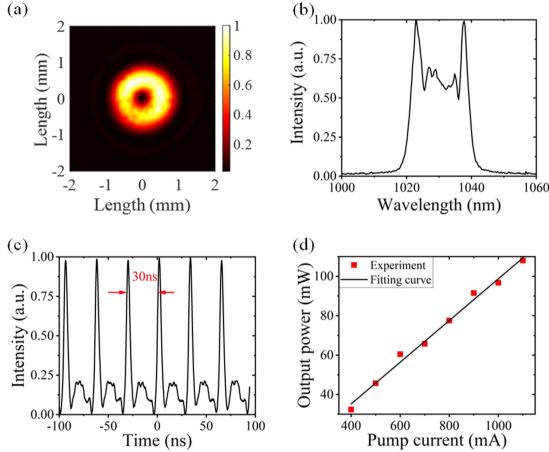| Optical elements	Jones Matrix	Parameters
QWP	$G_{\pm 45°} = \begin{bmatrix} 1 & \mp i \\ \mp i & 1 \end{bmatrix}$	$\lambda/4$ wave plate with its fast axis set at $\alpha = \pm 45°$
VWP	$G_v = \begin{bmatrix} \cos\theta & \sin\theta \\ \sin\theta & -\cos\theta \end{bmatrix}$	the azimuth angle θ (see Fig. 1(b) inset for the schematic of VWP)

Fig. 2.   Characterization of mode-locked OAM laser. (a) Spatial profile of the laser output after pulse compression. (b) Spectrum of the mode-locked laser. (c) Pulse train profile. (d) Relationship between the average output power and pump current.

beam γ is evaluated by (4) [34]. I_1 represents the intensity of the perfect vortex beam and I_2 is the experimental measured beam profile (Fig. 2(a)). I_1 and I_2 are the average values of I_1 and I_2. The final purity index γ of 97.6% can be obtained.

$$\gamma = \frac{\sum \left(I_1 - \bar{I}_1\right)\left(I_2 - \bar{I}_2\right)}{\sqrt{\sum \left(I_1 - \bar{I}_1\right)^2}\sqrt{\sum \left(I_2 - \bar{I}_2\right)^2}} \qquad (4)$$

Fig. 2(b) shows the output spectrum of the laser. The spectrum has a signature spectral profile of an ANDi fiber laser with a 3-dB bandwidth of 18 nm centered at 1030nm. Fig. 2(c) shows the pulse train profile measured by a photo detector. The interval between two pulses is 30ns, corresponding to a repetition rate of 33 MHz. Fig. 2(d) shows the average output power of the laser when the pump current increases from 400mA to 1200mA. The average output power has maximum value of 108 mW, corresponding to a pulse energy of 3.3 nJ.

The center wavelength of the OAM laser can be continuously tuned from 1015 nm to 1038 nm by changing the diffraction angle of the grating. Fig. 3(a) plots the spectrum of the laser output when the pump current is fixed at 500mA. All spectra have a similar profile of an ANDi fiber laser. In the time domain, the pulse is linearly chirped to a pulse duration of $\sim$ 1ps. We
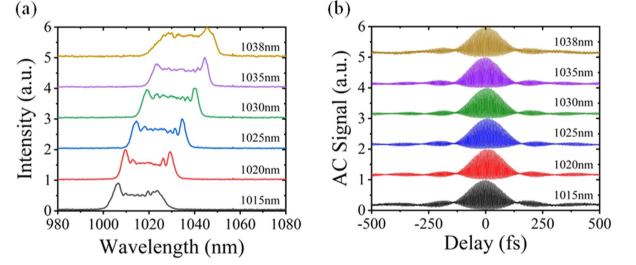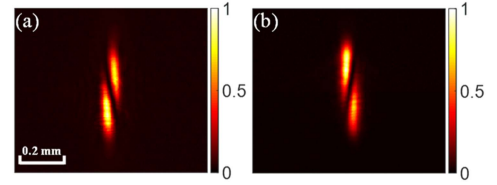

Fig. 3.   The mode-locking spectrum and the corresponding autocorrelation waveform are obtained by changing the tilt angle of the grating in the cavity. (a) Mode-locking spectra at different central wavelengths. (b) Interference autocorrelation waveform corresponding to the central wavelength.

Fig. 4.   CCD profile when the laser beam is focused by a cylindrical lens. (a) OAM laser with $\ell = +1$. (b) OAM laser with $\ell = -1$.

use a pair of grating to compress the pulse down to $\sim$100 fs. Fig. 3(b) shows the interferometric autocorrelation profile of the compressed pulse. The compressed pulse has a shortest pulse duration of 87 fs when the center wavelength of the laser is at 1035nm.

To confirm the vortex beam feature of this laser, we use a cylindrical lens to focus the laser beam into a CCD camera [35]. Fig. 4(a) shows the CCD profile when the OAM laser has a topological charge of $l = +1$. When the fast axis of QWP2-5 is rotated by 90°, the laser can emit vortex beam with an opposite topological charge. Fig. 4(b) shows the CCD profile when the OAM laser has a topological charge of $l = -1$.

IV. CONCLUSION

In conclusion, we demonstrate a wavelength-tunable and OAM-switchable mode-locked fiber laser that can directly emit outputs in the form of vortex beam. The laser has a typical ANDi fiber laser structure with additional polarization control elements for realizing the modal conversion inside the cavity. Both the center wavelength and OAM can be switched by changing the diffraction grating and polarization controlling elements inside the laser while the mode-locking state is always retained during the process. By replacing the intracavity vortex wave plates (VWP) with higher order VWPs, the laser can generate vortex beam with higher topological charges as well. Moreover, the concept of building such OAM ultrafast laser can be further expanded to build mode-locked laser that emits output with even more sophisticated spatial profiles. This compact, wavelength-tunable and OAM-switchable ultrafast fiber laser has broad application prospects in ultrafast optical fields such as space communication technology, ultra-laser processing and super-resolution imaging.

REFERENCES

[1] Q. W. Zhan, "Cylindrical vector beams: From mathematical concepts to applications," *Adv. Opt. Photon.*, vol. 1, no. 1, pp. 1–57, Jan. 2009.

[2] F. O. Fahrbach, P. Simon, and A. Rohrbach, "Microscopy with self-reconstructing beams," *Nature Photon.*, vol. 4, no. 11, pp. 780–785, Nov. 2010.

[3] Z. Bouchal, J. Wagner, and M. Chlup, "Self-reconstruction of a distorted nondiffracting beam," *Opt. Commun.*, vol. 151, no. 4–6, pp. 207–211, Jun. 1998.

[4] S. Bernet, A. Jesacher, S. Furhapter, C. Maurer, and M. Ritsch-Marte, "Quantitative imaging of complex samples by spiral phase contrast microscopy," *Opt. Exp.*, vol. 14, no. 9, pp. 3792–3805, May 2006.

[5] S. Furhapter, A. Jesacher, S. Bernet, and M. Ritsch-Marte, "Spiral phase contrast imaging in microscopy," *Opt. Exp.*, vol. 13, no. 3, pp. 689–694, Feb. 2005.

[6] M. Padgett and R. Bowman, "Tweezers with a twist," *Nature Photon.*, vol. 5, no. 6, pp. 343–348, Jun. 2011.

[7] T. Zuchner, A. V. Failla, and A. J. Meixner, "Light microscopy with doughnut modes: A concept to detect, characterize, and manipulate individual nanoobjects," *Angewandte Chem.-Int. Ed.*, vol. 50, no. 23, pp. 5274–5293, 2011.

[8] D. G. Grier, "A revolution in optical manipulation," *Nature*, vol. 424, no. 6950, pp. 810–816, Aug. 2003.

[9] A. E. Willner et al., "Optical communications using orbital angular momentum beams," *Adv. Opt. Photon.*, vol. 7, no. 1, pp. 66–106, Mar. 2015.

[10] N. Bozinovic et al., "Terabit-scale orbital angular momentum mode division multiplexing in fibers," *Sci.*, vol. 340, no. 6140, pp. 1545–1548, Jun. 2013.

[11] J. Leach et al., "Quantum correlations in optical angle-orbital angular momentum variables," *Sci.*, vol. 329, no. 5992, pp. 662–665, Aug. 2010.

[12] V. Arrizon, U. Ruiz, R. Carrada, and L. A. Gonzalez, "Pixelated phase computer holograms for the accurate encoding of scalar complex fields," *J. Opt. Soc. Amer. A-Opt. Image Sci. Vis.*, vol. 24, no. 11, pp. 3500–3507, Nov. 2007.

[13] H. Sroor et al., "High-purity orbital angular momentum states from a visible metasurface laser," *Nature Photon.*, vol. 14, no. 8, pp. 498–503, Aug. 2020.

[14] Z. Bomzon, G. Biener, V. Kleiner, and E. Hasman, "Radially and azimuthally polarized beams generated by space-variant dielectric subwavelength gratings," *Opt. Lett.*, vol. 27, no. 5, pp. 285–287, Mar. 2002.

[15] S. C. Tidwell, D. H. Ford, and W. D. Kimura, "Generating radially polarized beams interferometrically," *Appl. Opt.*, vol. 29, no. 15, pp. 2234–2239, May 1990.

[16] L. Marrucci, C. Manzo, and D. Paparo, "Optical spin-to-orbital angular momentum conversion in inhomogeneous anisotropic media," *Phys. Rev. Lett.*, vol. 96, no. 16, Apr. 2006, Art no. 163905.

[17] A. Forbes, "Structured light from lasers," *Laser Photon. Rev.*, vol. 13, no. 11, Nov. 2019, Art no. 1900140.

[18] Z. Dong, H. Sun, Y. Zhang, J. Zou, L. Xu, and Z. Luo, "Visible-wavelength-tunable, vortex-beam fiber laser based on a long-period fiber grating," *IEEE Photon. Technol. Lett.*, vol. 33, no. 21, pp. 1173–1176, Nov. 2021.

[19] K. Toyoda et al., "Transfer of light helicity to nanostructures," *Phys. Rev. Lett.*, vol. 110, no. 14, Apr. 2013, Art no. 143603.

[20] K. Toyoda, K. Miyamoto, N. Aoki, R. Morita, and T. Omatsu, "Using optical vortex to control the chirality of twisted metal nanostructures," *Nano Lett.*, vol. 12, no. 7, pp. 3645–3649, Jul. 2012.

[21] C. Varin et al., "Direct electron acceleration with radially polarized laser beams," *Appl. Sci.-Basel*, vol. 3, no. 1, pp. 70–93, Mar. 2013.

[22] D. S. Simon and A. V. Sergienko, "Two-photon spiral imaging with correlated orbital angular momentum states," *Phys. Rev. A*, vol. 85, no. 4, Apr. 2012, Art no. 043825.

[23] H. Chen et al., "High-power, femtosecond vortex beams generation in the visible and near-infrared region," *J. Lumin.*, vol. 248, Aug. 2022, Art no. 118949.

[24] K. Huang, J. Zeng, J. W. Gan, Q. Hao, and H. P. Zeng, "Controlled generation of ultrafast vector vortex beams from a mode-locked fiber laser," *Opt. Lett.*, vol. 43, no. 16, pp. 3933–3936, Aug. 2018.

[25] Y. Y. Hu et al., "Controlled generation of mode-switchable nanosecond pulsed vector vortex beams from a Q-switched fiber laser," *Opt. Exp.*, vol. 30, no. 18, pp. 33195–33207, Aug. 2022.

[26] D. Lin, Y. T. Feng, Z. Q. Ren, and D. J. Richardson, "The generation of femtosecond optical vortex beams with megawatt powers directly from a fiber based Mamyshev oscillator," *Nanophoton.*, vol. 11, no. 4, pp. 847–854, Feb. 2022.

[27] J. F. Lu et al., "Real-time observation of vortex mode switching in a narrow-linewidth mode-locked fiber laser," *Photon. Res.*, vol. 8, no. 7, pp. 1203–1212, Jul. 2020.

[28] Z. C. Zhang, S. Wang, X. W. Hu, B. G. Wang, and J. Wang, "Ultrafast ytterbium-doped all-fiber laser with vortex pulse emissions," *Laser Phys. Lett.*, vol. 19, no. 3, Mar. 2022, Art. no. 035103.

[29] Z. M. Zhang et al., "All-fiber short-pulse vortex laser with adjustable pulse width," *Laser Phys.*, vol. 30, no. 5, Apr. 2020, Art. no. 055102.

[30] C. Y. Ma, A. Khanolkar, and A. Chong, "High-performance tunable, self-similar fiber laser," *Opt. Lett.*, vol. 44, no. 5, pp. 1234–1236, Mar. 2019.

[31] A. Chong, J. Buckley, W. Renninger, and F. Wise, "All-normal-dispersion femtosecond fiber laser," *Opt. Exp.*, vol. 14, no. 21, pp. 10095–10100, Oct. 2006.

[32] K. Lingjie, X. Xiaosheng, and Y. Changxi, "Tunable all-normal-dispersion Yb-doped mode-locked fiber lasers," *Laser Phys.*, vol. 20, no. 4, pp. 834–837, Apr. 2010.

[33] Y. W. Zhao, J. T. Fan, H. S. Shi, Y. P. Li, Y. J. Song, and M. L. Hu, "Intracavity cylindrical vector beam generation from all-PM Er-doped mode-locked fiber laser," *Opt. Exp.*, vol. 27, no. 6, pp. 8808–8818, Mar. 2019.

[34] M. Lyu, Z. Q. Lin, G. W. Li, and G. H. Situ, "Fast modal decomposition for optical fibers using digital holography," *Sci. Rep.*, vol. 7, Jul. 2017, Art no. 6556.

[35] S. N. Alperin, R. D. Niederriter, J. T. Gopinath, and M. E. Siemens, "Quantitative measurement of the orbital angular momentum of light with a single, stationary lens," *Opt. Lett.*, vol. 41, no. 21, pp. 5019–5022, Nov. 2016.